Chapter 5

Mitophagy-Related Cell Death Mediated by Vacquinol-1 and TRPM7 Blockade in Glioblastoma IV

Philip Sander, Paul Walther, Barbara Moepps, Michael Hinz, Haouraa Mostafa, Patrick Schaefer, Andrej Pala, C. Rainer Wirtz, Michael Georgieff and E. Marion Schneider

Additional information is available at the end of the chapter

http://dx.doi.org/10.5772/intechopen.77076

Abstract

Glioblastoma IV (GBM) is one of the deadliest malignant diseases in adults and is characterized by a high mutation rate and multiple traits to suppress inborn and acquired immunity. We here approached autophagy-related cell death in newly established GBM cell lines derived from individual tumor isolates. Treatment with a small molecule, termed Vacquinol-1 (Vac) exhibited 100% GBM cell death, which was related to mitochondrial dysfunction, calcium-induced endoplasmic reticulum (ER)-stress, and autophagy. The toxicity of Vac was significantly increased by the inhibition of transient receptor potential cation channel, subfamily M, member 7 (TRPM7). TRPM7 is overexpressed in GBM as well as in many other tumors and thus may be a potential target by the natural compound carvacrol. Of note, at higher concentrations, Vac also induced growth inhibition and cell death in non-transformed cell types. However, in the presence of the TRPM7 inhibitor carvacrol, the tumor-selective effect of Vac was very much increased. Results given in the present study are based on long-term video microscopy using IncuCyteZOOM®, calcium measurements, and 3D ultrastructural analysis using the cryofixed material.

Keywords: glioblastoma IV (GBM), Vacquinol-1, TRPM7, carvacrol, calcium, endoplasmic reticulum (ER)-stress, autophagy, mitochondria, mitophagy, cell death, 3D cryoelectron microscopy

1. Introduction

The search for better tumor treatments in glioblastoma (GBM) and other cancers is ongoing. Recently, a major step forward has been achieved on the basis of immune interventions. Specifically, humanized antibodies directed against immune checkpoint antigens are now available to reconstitute immune recognition of the malignant cell in vivo [1]. In addition to the ongoing search for novel checkpoint interventions, chimeric T cell antigen receptors recognizing clonal neoantigens of a given malignancy are promising candidates for an individualized approach [2]. For a broader range of tumors, however, the identification of novel chemotherapeutic drugs [2], potentially resulting in reduced tumor mass as well as improved stimulation of antigen presentation [3], and remain to be of high interest. In this context, we have been intrigued by the original observations of a small synthetic molecule, named Vacquinol-1, and its capacity to fulminant induce cell death in GBM. Even though the original description has been retracted due to non-reproducibility of the in-vivo data (http://retractionwatch.com/2017/07/20/not-want-create-false-hope-authors-retract-cell-paper-cant-replicate/), we here report novel findings on using Vacquinol-1 (here termed: Vac). The synthetic small molecule Vac appears to impair the hydrostatic balance of a tumor cell and induces vacuolization ending in cell rupture. The small therapeutical concentration window of action by Vac limits its application due to a cascade of side effects to occur in vivo [4, 5]. Interestingly, we recently reported that the discriminative effect by Vac against glioma, as opposed to non-transformed tissues could be increased in the presence of a plant derivative, carvacrol [6], likely acting by inhibiting TRPM7 [7]. We here provide evidence for a mechanism on Vac-induced cell death by deteriorating the mitochondrial membrane potential, increasing high intracellular calcium levels combined with endoplasmic reticulum (ER)-stress [8] and impaired calcium storage, followed by mitophagy and rupture of lysosomes and autophagolysosomes. Lysosomal rupture seems to constitute the final event leading to cell death by hydrostatic pressure-associated rupture of autophagolysosomes and the plasma membrane. The decisive effect of Vac against transformed vs. non-transformed tissues may be explicable by the functional sensitivity of TRPM7 to carvacrol in glioma. Essential aspects proving ER-stress and mitochondrial dysfunction have been unraveled by using 3D cryoelectron microscopy.

2. Results and discussion

We here extended our previous work on Vac sensitivity in 2 glioma cell lines (#12537-GB, U-87), and non-transformed dental pulp stem cells (DPSCs) [6], to a total of 7 other glioma cell lines, two fibroblast cell cultures and bone marrow stroma cell isolates. Using IncuCyteZOOM® long-term video microscopy, we determined Vac concentrations resulting in half-maximal cell death (inhibitory concentration: IC50) after 24 h. Accordingly, IC50 values for Vac to result in 50% cell death after 24 h ranged between 7.7 and 12.2 μM Vac in glioma cell lines, whereas non-transformed cells (fibroblasts, bone marrow stroma, and DPSCs) were less sensitive to Vac, resulting in IC50 values between 9.5 and 22.5 μM Vac. For further studies, we focused on two glioma cell lines with high (#12537-GB, IC50 = 8.2 μM), and low Vac sensitivity, respectively (#12794-GB; IC50 = 10.2 μM), indicating a more resistant phenotype. In the presence of the natural compound

http://dx.doi.org/10.5772/intechopen.77076

carvacrol, Vac-induced cell death was found to be increased in #12537-GB, as previously reported [6], an observation corresponding to the lower proliferative and less invasive phenotype of GBM when carvacrol was administered [7]. Carvacrol has been demonstrated to inhibit the transient receptor potential cation channel, subfamily M, member 7 (TRPM7 [7, 9], explaining the higher sensitivity of Vac-induced toxicity to the glioma cell line #12537-GB [6]. The gene encoding TRPM7 functions as both: An ion channel and a protein kinase [7]. In our experimental set-up, the addition of carvacrol at concentrations of 100 μM selectively increased the sensitivity to Vac-induced toxicity in our glioma cell lines, but not in non-transformed fibroblasts. To determine cell viability of pre-established cell layers, we applied the live cell imaging system IncuCyteZOOM® equipped with a 20× objective. Propidium-iodide staining was used to identify and count dead cells in a time-dependent manner. As shown in **Figure 1A**, high Vac concentrations >10 μM led to rapid cell death in both GBM cell lines as well as in non-malignant fibroblasts; 7 μM Vac resulted in significant cell death in #12537-GB cells (**Figure 1A**) after 12 h of incubation but not in #12794-GB cells (**Figure 1B**) and non-transformed fibroblasts (**Figure 1C**). The influence of carvacrol on Vac-induced cell death in glioma cell lines is shown in **Figure 1D** (#12537-GB), and **Figure 1E** (#12794-GB), and non-transformed fibroblasts (Hs68-Fi) in **Figure 1F**. After 56 h, carvacrol (100 μM) significantly (Sidak's Post hoc test after two-way ANOVA; p-values between 0.0198 and 0.0001) enhanced Vac-induced cell death in #12794-GB but not in non-transformed fibroblasts (**Figure 1D–F**). Accordingly, only glioma cell lines and not fibroblasts increased their sensitivity against Vac in the presence of carvacrol. To understand the action by carvacrol acting on TRPM7, we performed calcium measurements of glioma cells upon Vac stimulation with and without carvacrol pre-incubation. **Figure 2** demonstrates a rapid loss of cytoplasmic calcium in both GBM cell lines followed by subsequently elevated calcium levels. The addition of ionomycin was included at the end of the experiment to test the residual capacity of the target cell to mount a calcium response. This ionomycin-induced calcium peak was higher in #12537-GB than in #12794-GB. When carvacrol was present, Vac-treatment caused a rapid loss of cytoplasmic calcium again in both cell lines. However, the Vac-induced loss of cytoplasmic calcium was not followed by an increased cytoplasmic calcium level (**Figure 2C** and **D** cf. **Figure 2A** and **B**). The latter might have been due to the inhibition of TRPM7 and loss of control of store-operated calcium channels (SOCEs). Along with this line, Faouzi et al. recently, described the regulation of SOCEs by the kinase activity of TRPM7 [10]. As a consequence, blockade of the TRPM7 would lead to an impaired reconstitution of calcium sequestration to cytoplasmic stores [10].

The molecular events by Vac affecting lipid bilayer integrity and its proton catching properties may contribute to dysfunction of calcium-storage organelles, such as ER and mitochondria. In the end, Vac appears to transiently affect the integrity of lipid bilayers in calcium storage organelles, resulting in transient leakage of bivalent cations such as calcium (**Figure 2**). The partial reconstitution of membrane integrity in the presence of Vac in the range of IC50 values appears to be significantly impaired in the presence of the TRPM7 blocker, carvacrol. As a consequence, calcium influx from external medium would be inhibited [10] and thereby lead to impaired calcium sequestration by ER and mitochondria. In the end, calcium measurements proved, that carvacrol appears to be essential to block endogenous membrane reconstitution. The observations of the combined effects by Vac and carvacrol remind of results obtained in a study performed with curcumin, which was tested on cell death in a melanoma cell line. Bakhshi and colleagues found a dramatic increase of ER-induced cell stress in curcumin-treated melanoma

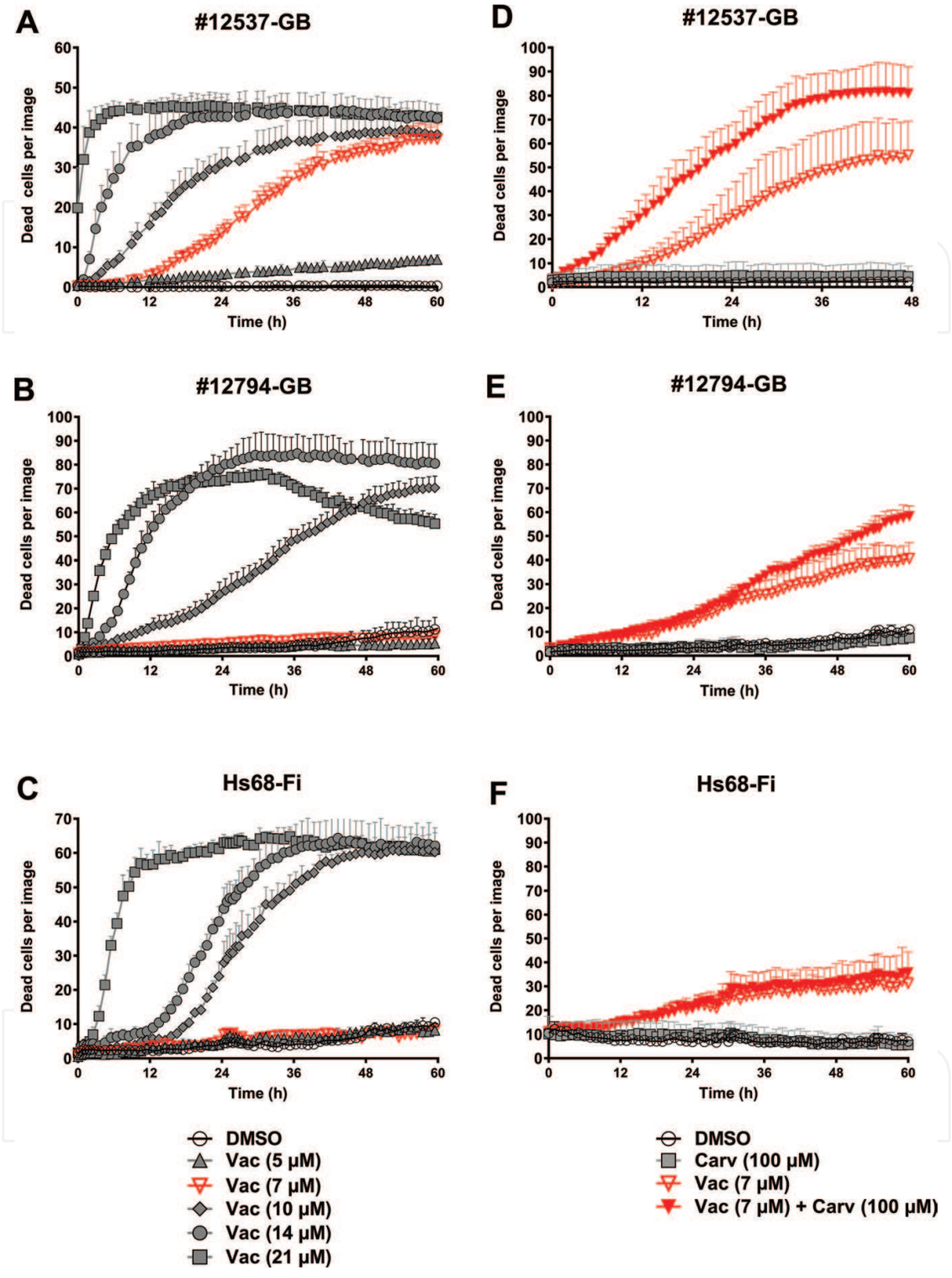

Figure 1. Cell death induced by Vac in the absence and presence of carvacrol. Kinetics of cell death were determined from the PI-positive (dead) cells displayed as red object count/image (y-axis). #12537-GB, #12794-GB, and Hs68 were followed for 60 h (x-axis) (IncuCyteZOOM®). The cells were treated either with DMSO (vehicle control), 5, 7, 10, 14, or 21 µM Vac. All values are means ± SD (biological triplicates) (A–C). Semi-confluent #12537-GB, #12794-GB, or Hs68 were treated with DMSO (vehicle control) or Vac (7 µM) in the presence or absence of 100 µM carvacrol. #12537-GB were followed for 48 h, and #12794-GB, and Hs68 were followed for 60 h (x-axis) (IncuCyteZOOM®). All values are means ± SD (#12537-GB: six biological replicates; #12794-GB and Hs68-Fi: biological triplicates) (D–F). All imaging was performed using IncuCyteZOOM® at 20× objective.

http://dx.doi.org/10.5772/intechopen.77076

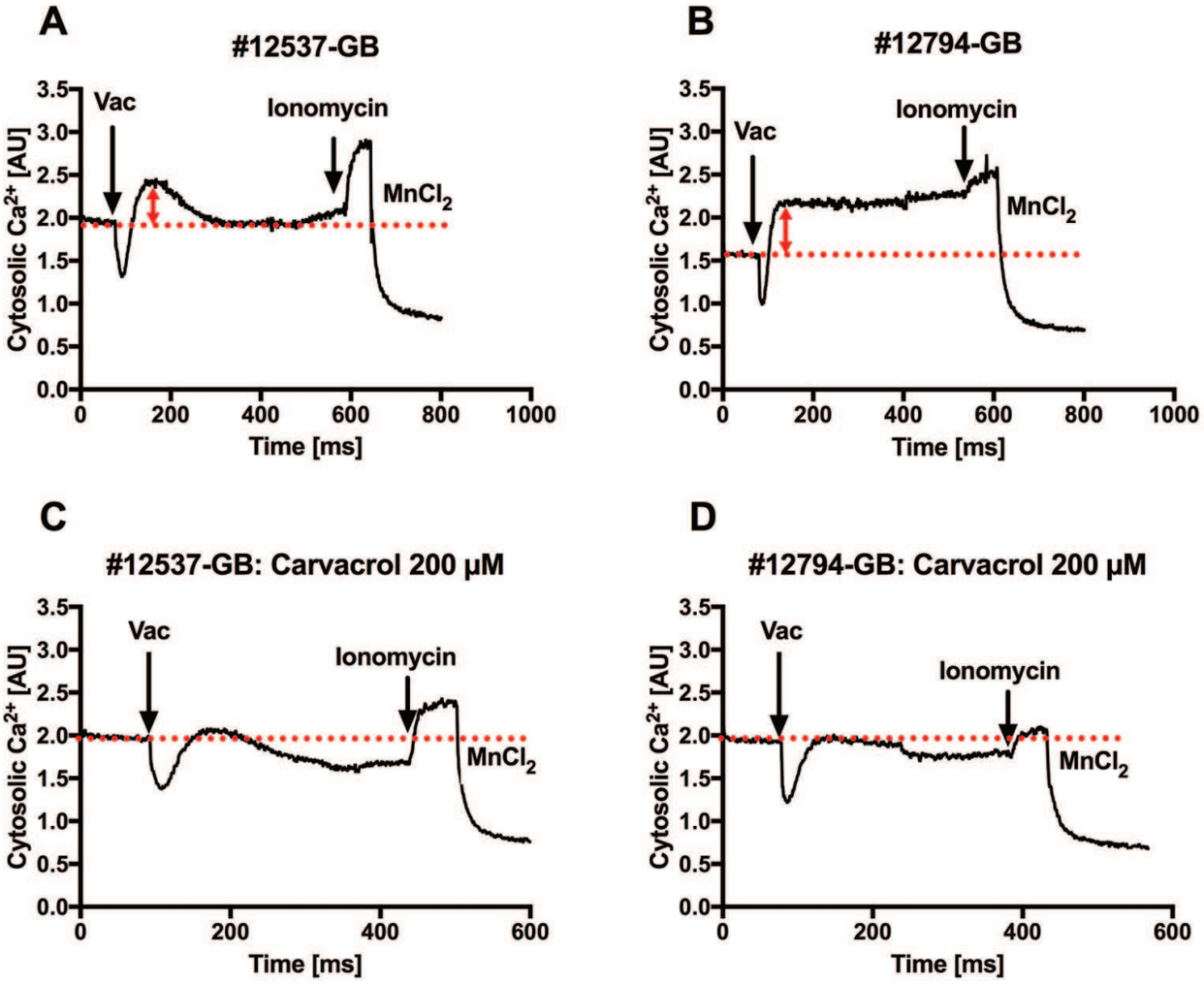

Figure 2. Calcium signaling in GBM cell lines in presence and absence of carvacrol. Calcium responsiveness was tested in Fura-2 (Thermofisher.com)-labeled #12537-GB cells or #12794-GB cells using a LS55 luminescence spectrometer (PerkinElmer.com). After labeling, cells were diluted in HBSS (Hank's balanced salt solution) at a cell concentration of 1×10^6 per ml. The cells were pretreated with DMSO (vehicle control) (A and B) or 200 µM carvacrol for 1 h (C and D). Upon suspension in the cuvette of the spectrometer, suspension cells were stimulated with Vac 7 µM followed by ionomycin (1 µM, Sigma.com). At the end of the experiment, the Fura-2 signal was quenched using $MnCl_2$. Results are given as relative fluorescence ([AU], arbitrary units) and are representative for two independent experiments. The red dashed line emphasizes increased cytoplasmic calcium levels following the calcium depletion induced by Vac (A and B), which is absent after carvacrol pre-incubated cell suspensions (C and D).

cells an effect, which appeared to overrun the chronically active cytoprotection of a malignant, chronically stressed cell type [11]. In contrast to non-transformed tissues, cancer cells are dependent on chronic stress pathway activation [11]. The effector of cell death mediated by curcumin appeared to be due to the massive and acute stress by a curcumin-inducible down-regulation of the protective stress proteins. Curcumin is expected to inhibit the ATPase pump and similarly to carvacrol in GBM, may lead to increased cytoplasmic calcium concentrations. Again, ER-stress appears to contribute to impaired membrane integrity and allows calcium to freely enter the cells. Under conditions of the blocked sequestration of calcium to mitochondria and ER, this effect is expected to be even more dramatic to the target tissue [11]. Pathway analysis proved ER-stress related cell death in this melanoma model. As a consequence, the

authors hypothesized that mechanisms over activating stressors in malignant cells may be crucial for innovative approaches in cancer therapy [11]. In the case of Vac, a mechanism of impaired mitochondrial calcium sequestration is likely due to uncoupling of oxidative phosphorylation by Vac, which has been accurately investigated and described by Feng and colleagues [12]. Uncoupling of mitochondria results in a collapse of the mitochondrial membrane potential (ΔΨm), which may explain the loss of mitochondrial membrane integrity. To assess whether Vac influences ΔΨm in GBM, we used the cyanine dye JC-1 (5, 50, 6, 60-tetrachloro-1, 10, 3, 30 tetraethylbenzimidazolocarbo-cyanine iodide) forming J-aggregates in mitochondria with high ΔΨm spectrally distinguishable from dye monomers at lower ΔΨm [13]. JC-1 monomers emit green fluorescence with a maximum at 530 nm (green), whereas J-aggregates emit orange-red fluorescence with a maximum at 595 nm (orange-red). After 4 h treatment, Vac leads to a significant decrease in the ratio of red/green fluorescence indicating a collapse of the ΔΨm (**Figure 3A**). In summary, the reduction of ΔΨm upon Vac treatment emphasizes the uncoupling properties of Vac as previously described by Feng and colleagues [12].

Moreover, the detrimental process in Vac treated GBM cells occurs in parallel with the upregulation of autophagy, which has been addressed by using an amphiphilic tracer CytoID®. CytoID® stains lysosomes minimally while maximizing the fluorescence of autophagosomes [14]. Using the CytoID® autophagy detection kit (**Figure 3B**), we found increased green fluorescence indicating upregulation of autophagy upon 4 h Vac treatment. These results correspond to upregulation of LC3-II determined by Western-Blot (data not shown). Reactive oxygen species formation (ROS) was also upregulated by Vac treatment as demonstrated in **Figure 3C**. Carboxy-H_2DCFDA is non-fluorescent but in the presence of ROS, when this reagent is oxidized, it becomes green fluorescent [15]. The overall proof of Vac-induced pathology in GBM is here provided by 3D cryoelectron microscopy (**Figure 4**). The screenshot of the 3D tomogram performed from GBM during constitutive culture shows occasional mitophagy, occurring by phagophore formation and subsequent digestion in autophagolysosomes (**Figure 4A**). In addition, relatively high numbers of autophagolysosomes, sparse microtubules, and unorganized actin filaments are present ([16], **Figure 4A**, untreated #12537-GB). By contrast, GBM, treated with Vac for 4 h differ by the following parameters: Identification of (i) massive stress fiber formation, (ii) formation of actin bundles attached to bent mitochondria, and (iii) impressively enlarged cisternae of ER, which indicates ER-stress (**Figure 4B**, 4 h Vac-treated #12537-GB). Moreover, the autophagolysosomes contain electron dense structures, which were structurally compatible with the partially digested mitochondrial material (**Figure 4B**, white arrows). The autophagolysosomes almost never showed a double lipid bilayer, which may indicate that the outer mitochondrial membrane might have been involved in the formation of autophagosomes, as previously described [17]. In the accompanying tomogram (https://mts.intechopen.com/download/index/process/155/authkey/5fc95d7040949214f944031367b18403), a Vac-treated #12537-GB cell has been analyzed from an area in the vicinity of the nucleus. This tomogram shows an elongated, bent mitochondrion, attached to a bundle of active fibers, which appear to be involved in bending (or even traction?) of the organelle. The ER is very close to the mitochondrion with enlarged cisternae, a characteristic of stressed cells as previously demonstrated. This tomogram also shows that the number of autophagolysosomes is dramatically increased when compared to the non-treated #12537-GB (cf. supplementary video I in Gorbunov and Schneider [16]). Finally,

http://dx.doi.org/10.5772/intechopen.77076

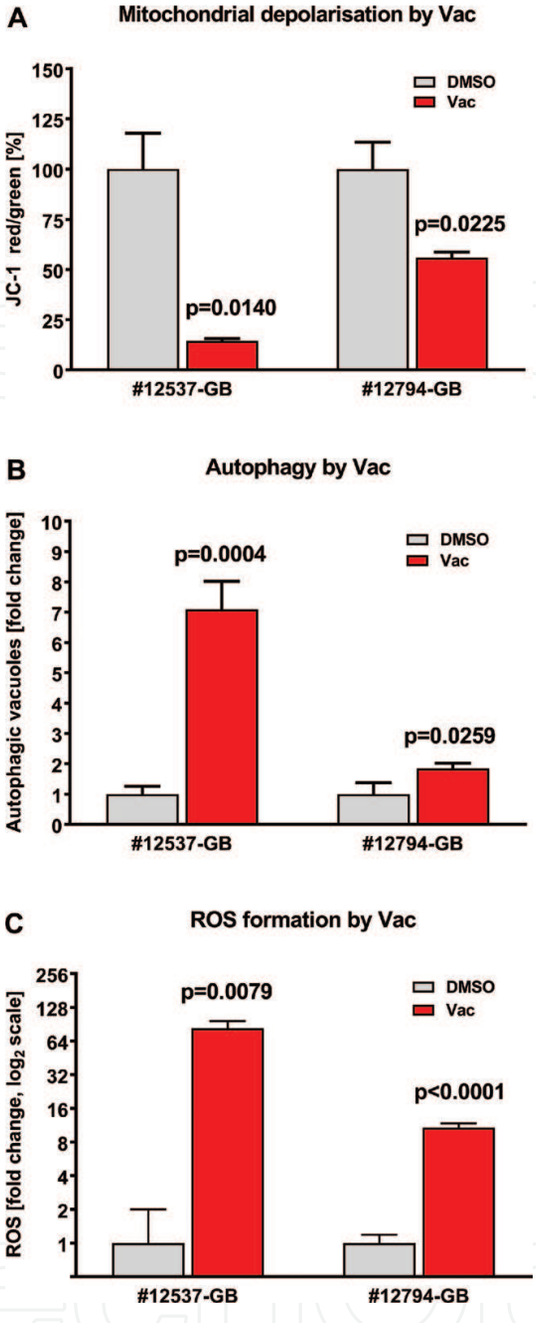

Figure 3. Vac induces autophagy/mitophagy in GBM cells, induces ROS formation and leads to a decrease in ΔΨm. Semi-confluent #12537-GB or #12794-GB cells were stained with JC-1 (2 μg/ml). JC-1 stained cells were treated with DMSO (vehicle control) or 7 μM Vac for 4 h. Quantitative analysis of the ratio red/green fluorescence. Vac leads to a decrease in the ratio red/green in #12537-GB ($p = 0.014$, t-test) as well as #12794-GB ($p = 0.0225$, t-test) indicating a collapse of the ΔΨm. All values are mean values of the total red/green integrated fluorescence intensity per image ± SD (biological triplicates). Data were normalized to the corresponding control (100%) (A). Semi-confluent #12537-GB cells were treated with DMSO (vehicle control) or 7 μM Vac for 4 h. After incubation, cells were stained with the green-fluorescent autophagosome/autophagolysosome dye CytoID®. Quantitative analysis of autophagic vacuoles (fold change compared to DMSO control). Vac leads to an increase in autophagic vacuoles in #12537-GB cells as well as in #12794-GB cells ($p = 0.0004$ and $p = 0.0259$, respectively, t-test). All values are mean values of the green object count ± SD (biological triplicates). Data were normalized to the respective control (B). Semi-confluent #12537-GB or 12794-GB cells were treated with DMSO (vehicle control) or 7 μM Vac for 4 h. After incubation, cells were stained with CM-H_2DCFDA (green fluorescent) to detect ROS. Quantitative analysis of ROS production after 4 h in #12537-GB or #12794-GB. Vac leads to an increased ROS production in #12537-GB ($p = 0.0079$, t-test) as well as #12794-GB ($p < 0.0001$, t-test), (C). All values are mean values of the total green integrated fluorescence intensity per image ± SD (biological triplicates). Data were normalized to the corresponding control. All images were obtained using IncuCyteZOOM® equipped with a 20× objective.

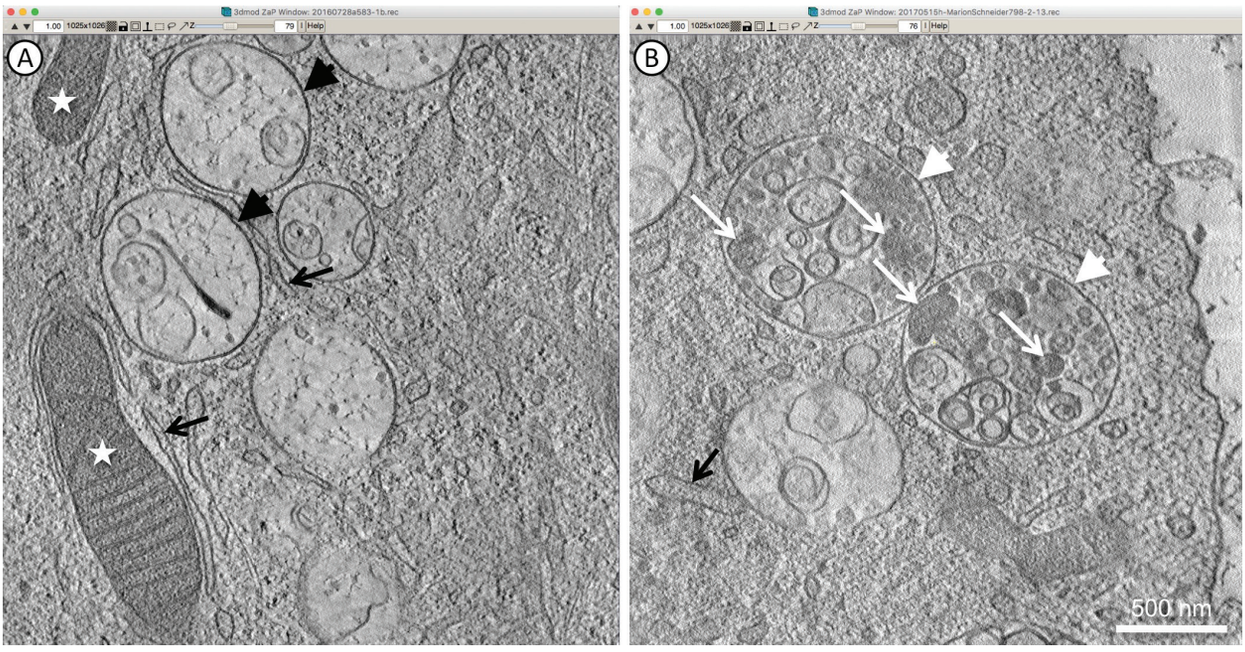

Figure 4. Ultrastructural changes induced by Vac in GBM cells (#12537-GB). Virtual sections of #12537-GB cells investigated by STEM tomography demonstrate active mitophagy in control cells with early phagophore formation around mitochondria (white stars) by smooth ER cisternae (black arrows); in addition, numerous autophagolysosomes (black arrowheads) are shown with fully digested cytoplasmic as well as organelle derived material (A), this video section is part of the video tomogram provided as supplementary file 1 [16]; following Vac-treatment (4 h, 7 μM), phagophore formation is not prominent, ER appears to be swollen (black arrow as an example), and autophagolysosomes (white arrowheads) are more abundant. The material ingested is not fully digested, residual mitochondria can be identified by their morphological remnants (white arrows) (B). https://mts.intechopen.com/download/index/process/155/authkey/5fc95d7040949214f944031367b18403.

the massively upregulated mitophagy in 4 h Vac-treated GBM does not appear to occur with microtubule-assisted mitochondrial fission, as demonstrated in stressed tumor cells [18] since microtubules appear to be randomly distributed (https://mts.intechopen.com/download/index/process/155/authkey/5fc95d7040949214f944031367b18403).

3. Materials and methods

3.1. Cell lines and cell culture

The glioma cell line #12537-GB has been previously described [6]. The #12794-GB cell line has been established from a female patient's tumor material received from the neurosurgical department of the Bezirkskrankenhaus in Günzburg (Universal trial number: U111-1179-3127) with patient-informed consent. The tumor material was minced and cells from the tumor material were taken into the culture by trypsinization of the tumor material (2.5% trypsin), followed by Ficoll separation. Continuous cultures were performed in Iscove's Modified Dulbecco's Medium (IMDM) (Lonza.com, USA) supplemented with 10% fetal calf serum (FCS, endotoxin-free, Batch 0247x, Merck/Biochrom.com, Germany), GlutaMAX (ThermoFisher.com, USA), and antibiotics at 37°C under 5% CO_2. Hs68 fibroblasts (Hs68-Fi) were purchased from ATCC, and cultured in IMDM containing 10% endotoxin-free FCS (Batch No: 0247x, Merck/Biochrom.com).

http://dx.doi.org/10.5772/intechopen.77076

3.2. Ethical statement

The work with human GBM material/cell lines has been approved by the local Ethics Committee of the University Hospital Ulm (universal trial number: U111-1179-3127) with patient-informed consent.

3.3. Analysis of cell death by IncuCyteZOOM®

Cells were seeded into flat-bottom 96-well microtiter plates (Sarstedt.com, Germany) (density: 17,000 cells per cm^2). Semi-confluent cell layers were treated one day after seeding with DMSO (vehicle control) or Vac (Selleckchem.com, Germany; Stock: 76 mM in DMSO) in the presence of 10 μg/ml PI (Sigma.com, USA). Carvacrol was purchased from Sigma-Aldrich (Sigma.com, USA). Cell death was quantified as the red object count/image by the IncuCyteZOOM® software.

3.4. Detection of autophagy/mitophagy using Cyto-ID® staining

Staining of autophagic vacuoles was performed using the CytoID® autophagy detection kit (Enzolifesciences.com, Germany). GBM cells were seeded into flat-bottom 96-well microtiter plates (Sarstedt.com). One day after seeding, semi-confluent GBM cell layers were treated for 4 h with 0.01% DMSO (vehicle control) or 7 μM Vac to induce autophagy. After treatment, the culture medium was replaced by fresh culture medium containing CytoID® green detection reagent in a 10^{-3} dilution. After 15 min of incubation at 37°C, cells were washed twice in pre-warmed Hank's balanced salt solution (HBSS). Imaging was performed by IncuCyteZOOM®. Green object count reflecting autophagosomes/autophagolysosomes was quantified and collected by IncuCyteZOOM® software.

3.5. Detection of ROS

To detect ROS, carboxy-H_2DCFDA (CM-H_2DCFDA) (Thermofisher.com, USA) was used. In the presence of ROS, the dye gets oxidized and emits green fluorescence. GBM cells were seeded into flat-bottom 96-well microtiter plates (Sarstedt.com). One day after seeding, semi-confluent GBM layers were treated with 0.01% DMSO (vehicle control) or 7 μM Vac. After treatment, CM-H_2DCFDA (stock 5 mM in DMSO) was added in a final concentration of 5 μM to the culture medium (IMDM, 10%FCS). Imaging was performed by IncuCyteZOOM®. Total green fluorescence per image was quantified and collected by IncuCyteZOOM® software.

3.6. Evaluation of mitochondrial membrane potential using JC-1

To evaluate mitochondrial membrane potential, the dye JC-1 (5, 5′, 6, 6′-Tetrachloro-1, 1′, 3, 3′-tetraethyl-imidacarbocyanine iodide) was used (Thermofisher.com). In healthy mitochondria with high membrane potential, JC-1 forms red fluorescent aggregates. In contrast, JC-1 occurs as green fluorescent monomers in mitochondria with depolarized membrane potential. Semi-confluent GBM cell layers seeded into 24-well microtiter plates (Corning.com) (density: 17,000 cells per cm^2) were stained one day after culture with 2 μg/ml JC-1 for 30 min. After incubation, the culture medium was removed and cells were washed twice with pre-warmed HBSS. After

washing, the fresh culture medium was added and cells were treated for 4 h with 0.01% DMSO (vehicle control) or 7 μM Vac. Imaging was performed by IncuCyteZOOM® and red/green total fluorescence per image was quantified and collected using IncuCyteZOOM® software. The ratio between red and green fluorescence was calculated. A shift from red to green fluorescence and therefore, a decline in the red/green ratio indicates mitochondrial depolarization.

3.7. Electron microscopy

Sapphire discs (Engineering Office M. Wohlwend GmbH, Switzerland) were used as support for the adherent glioma cell culture. The 0.170 mm thick sapphire discs were carefully immersed in complete medium and the cells were seeded on top. A 50 μm gold spacer ring (diameter 3.05 mm, central bore 2 mm; Plano GmbH, Germany) was mounted in between two sapphire discs with the cells grown on them, similar to the protocol introduced by Hawes et al. [19]. These sandwiches were high-pressure frozen without aluminum planchettes and without the use of hexadecene. Freeze substitution was performed as described in Villinger et al. [20] with a substitution medium consisting of acetone with 0.2% osmium tetroxide, 0.1% uranyl acetate, and 5% water for 19 h. During this time period, the temperature was exponentially raised from 183 to 273 K. After substitution, the samples were maintained at room temperature for 30 min and then washed twice with acetone. After stepwise embedding of the samples in Epon (Fluka.com, USA) (polymerization at 333 K within 72 h), they were cut using a microtome (Leica Ultracut UCT ultramicrotome) with a diamond knife (Diatome, Switzerland) to semi-thin sections with a nominal thickness of 550 nm.

For STEM tomography, 550 nm semithin sections were coated with 25 nm gold particles serving as fiducial markers for alignment of the images to a tomogram. The tilt series was collected on a JEM-2100F electron microscope operated at an acceleration voltage of 200 kV in the scanning transmission mode. Electron micrographs were recorded with a bright-field detector at a pixel size of 2.74 nm. A tilt-series was recorded from −72° to +72° at increments of 1.5°. The tomogram was created out of 97 images using the IMOD software package. Images were first aligned to an image stack and then computationally reconstructed using a weighted back-projection algorithm to form the tomogram [20].

3.8. Statistical analysis

Statistical analysis was performed using GraphPadPrism v7 (Graphpad.com, USA). To identify significant differences of endpoint analyzes, an unpaired two-tailed t-test was used. P-values are given in the respective graphs (column with the treatment). In case of kinetics, two-way ANOVA followed by Sidak's correction for multiple comparison. Multiplicity adjusted p-values are given. Observations with $p < 0.05$ were considered as significant.

Acknowledgements

We thank the International Graduate School in Molecular Medicine, Ulm University for supporting and evaluating HM, PS, and PSch. We are grateful to IntechOpen publisher for generous support to publish a virtual section of the supplementary file 1 in reference [16], as

Figure 4A (https://www.intechopen.com/books/autophagy-in-current-trends-in-cellular-physiology-and-pathology/introductory-chapter-overview-on-autophagy-in-burden-of-functions).

Conflict of interest

The authors declare no conflicts of interest.

Authors contributions

EMS drafted the manuscript (ms), PW performed STEM microscopy, 3D tomography and reconstruction, PS performed experiments, designed figures and contributed to the ms text; BM performed experiments and drafted the ms, MH, and PSch contributed to chemical property analysis of Vac, HM contributed to trans electron microscopy, AP, CRW, and MG edited the ms. All authors reviewed and approved the final version of the ms.

Author details

Philip Sander[1], Paul Walther[2], Barbara Moepps[3], Michael Hinz[4], Haouraa Mostafa[1], Patrick Schaefer[5], Andrej Pala[6], C. Rainer Wirtz[6], Michael Georgieff[1] and E. Marion Schneider[1]*

*Address all correspondence to: marion.schneider@uni-ulm.de

1 Department of Anesthesiology, University Hospital Ulm, Ulm, Germany

2 Central Facility for Electron Microscopy, University of Ulm, Ulm, Germany

3 Institute of Pharmacology and Toxicology, University Hospital Ulm, Ulm, Germany

4 M. Hinz UG, Neuried, Germany

5 Center for Mitochondrial and Epigenomic Medicine, Children's University Hospital of Philadelphia Research Institute, Philadelphia, PA, USA

6 Department of Neurosurgery, Bezirkskrankenhaus Günzburg, Günzburg, Germany

References

[1] Jendrossek V, Belka C, Bamberg M. Novel chemotherapeutic agents for the treatment of glioblastoma multiforme. Expert Opinion on Investigational Drugs. 2003;**12**:1899-1924. DOI: 10.1517/13543784.12.12.1899

[2] McGranahan N, Furness AJS, Rosenthal R, Ramskov S, Lyngaa R, Saini SK, Jamal-Hanjani M, Wilson GA, Birkbak NJ, Hiley CT, Watkins TBK, Shafi S, Murugaesu N, et al.

Clonal neoantigens elicit T cell immunoreactivity and sensitivity to immune checkpoint blockade. Science. 2016;**351**:1463-1469. DOI: 10.1126/science.aaf1490

[3] Emens LA, Middleton G. The interplay of immunotherapy and chemotherapy: Harnessing potential synergies. Cancer Immunology Research. 2015;**3**:436-443. DOI: 10.1158/2326-6066.CIR-15-0064

[4] Kitambi SS, Toledo EM, Usoskin D, Wee S, Harisankar A, Svensson R, Sigmundsson K, Kalderén C, Niklasson M, Kundu S, Aranda S, Westermark B, Uhrbom L, et al. Vulnerability of glioblastoma cells to catastrophic vacuolization and death induced by a small molecule. Cell. 2014;**157**:313-328. DOI: 10.1016/j.cell.2014.02.021

[5] Ahlstedt J, Förnvik K, Zolfaghari S, Kwak D, Lars GJ, Ernfors P, Salford LG, Redebrandt HN. Evaluating vacquinol-1 in rats carrying glioblastoma models RG2 and NS1. Oncotarget. 2018;**9**:8391-8399. DOI: 10.18632/oncotarget.23842

[6] Sander P, Mostafa H, Soboh A, Schneider JM, Pala A, Baron A-K, Moepps B, Wirtz CR, Georgieff M, Schneider EM. Vacquinol-1 inducible cell death in glioblastoma multiforme is counter regulated by TRPM7 activity induced by exogenous ATP. Oncotarget. 2017;**8**:35124-35137. DOI: 10.18632/oncotarget.16703

[7] Chen W-L, Barszczyk A, Turlova E, Deurloo M, Liu B, Yang BB, Rutka JT, Feng Z-P, Sun H-S. Inhibition of TRPM7 by carvacrol suppresses glioblastoma cell proliferation, migration and invasion. Oncotarget. 2015;**6**:16321-16340. DOI: 10.18632/oncotarget.3872

[8] Ozawa T. Modulation of ryanodine receptor Ca2+ channels (review). Molecular Medicine Reports. 2010;**2**:199-204. DOI: 10.3892/mmr-00000240

[9] Parnas M, Peters M, Dadon D, Lev S, Vertkin I, Slutsky I, Minke B. Carvacrol is a novel inhibitor of Drosophila TRPL and mammalian TRPM7 channels. Cell Calcium. 2009;**45**:300-309. DOI: 10.1016/j.ceca.2008.11.009

[10] Faouzi M, Kilch T, Horgen FD, Fleig A, Penner R. The TRPM7 channel kinase regulates store-operated calcium entry. The Journal of Physiology. 2017;**595**:3165-3180. DOI: 10.1113/JP274006

[11] Bakhshi J, Weinstein L, Poksay KS, Nishinaga B, Bredesen DE, Rao RV. Coupling endoplasmic reticulum stress to the cell death program in mouse melanoma cells: Effect of curcumin. Apoptosis. 2008;**13**:904-914. DOI: 10.1007/s10495-008-0221-x

[12] Feng X, Zhu W, Schurig-Briccio LA, Lindert S, Shoen C, Hitchings R, Li J, Wang Y, Baig N, Zhou T, Kim BK, Crick DC, Cynamon M, et al. Antiinfectives targeting enzymes and the proton motive force. Proceedings of the National Academy of Sciences. 2015;**1**:201521988. DOI: 10.1073/pnas.1521988112

[13] Perelman A, Wachtel C, Cohen M, Haupt S, Shapiro H, Tzur A. JC-1: Alternative excitation wavelengths facilitate mitochondrial membrane potential cytometry. Cell Death & Disease. 2012;**3**:e430-e437. DOI: 10.1038/cddis.2012.171 Nature Publishing Group

[14] Chan LLY, Shen D, Wilkinson AR, Patton W, Lai N, Chan E, Kuksin D, Lin B, Qiu J. A novel image-based cytometry method for autophagy detection in living cells. Autophagy. 2012;**8**:1371-1382. DOI: 10.4161/auto.21028

[15] Wu D, Yotnda P. Production and detection of reactive oxygen species (ROS) in cancers. Journal of Visualized Experiments. 2011;**3357**. DOI: 10.3791/3357

[16] Gorbunov NV, Schneider EM. Introductory chapter: Overview on autophagy in burden of functions. In: Gorbunov NV, Schneider EM, editors. Autophagy in Current Trends in Cellular Physiology and Pathology. IntechOpen; 2016. pp. 1-11. DOI: 10.5772/65435

[17] Cook KL, Soto-Pantoja DR, Abu-Asab M, Clarke PAG, Roberts DD, Clarke R. Mitochondria directly donate their membrane to form autophagosomes during a novel mechanism of parkin-associated mitophagy. Cell & Bioscience. 2014;**4**:16. DOI: 10.1186/2045-3701-4-16

[18] Wolf SG, Mutsafi Y, Dadosh T, Ilani T, Lansky Z, Horowitz B, Rubin S, Elbaum M, Fass D. 3D visualization of mitochondrial solid-phase calcium stores in whole cells. eLife. 2017; **6**:1-18. DOI: 10.7554/eLife.29929

[19] Hawes P, Netherton CL, Mueller M, Wileman T, Monaghan P. Rapid freeze-substitution preserves membranes in high-pressure frozen tissue culture cells. Journal of Microscopy. 2007;**226**:182-189. DOI: 10.1111/j.1365-2818.2007.01767.x

[20] Villinger C, Schaufl M, Gregorius H, Kranz C, Höhn K, Nafeey S, Walther P. Electron-Microscopy. 2014;**1117**:617-638. DOI: 10.1007/978-1-62703-776-1

IntechOpen